

Linear stability of two-dimensional flow to three-dimensional perturbations in a channel with a flexible wall

P. SIBANDA⁽¹⁾, S.S. MOTSA⁽²⁾, S. SHATEYI⁽³⁾

⁽¹⁾*School of Mathematical Sciences
University of KwaZulu-Natal,
P Bag X01 Scottsville 3209,
Pietermaritzburg, RSA*

⁽²⁾*Mathematics Department
University of Swaziland,
P Bag 4, Kwaluseni, Swaziland*

⁽³⁾*Department of Mathematics
Bindura University,
P Bag 1020, Bindura, Zimbabwe*

IN THIS PAPER we investigate the effects of three-dimensional disturbance waves on the stability of a two-dimensional channel flow with one compliant surface. The study exploits the multideck structure of the flow in the limit of large Reynolds numbers to make an asymptotic analysis of the flow and to derive linear neutral stability results. The study shows that for a flow over flexible surfaces, three-dimensional disturbances may be more unstable than two-dimensional modes for a given set of wall properties.

Key words: neutral stability, channel flow, compliant surface, asymptotic analysis.

1. Introduction

RELATIVELY FEW studies of the effects of three-dimensional disturbances on compliant wall stability have been conducted. The early studies, for example [1] and others (with a few exceptions such as [9]), were primarily concerned with the study of two-dimensional disturbances.

In [16], YEO offers two explanations for the apparent preoccupation with the study of two-dimensional disturbances in most of the investigations into the stability of boundary layer flow over compliant surfaces. He reasons that the relative simplicity in the formulation and analysis of two-dimensional disturbances may be a contributing factor but more importantly, according to the inviscid theory, the most unstable modes for a prescribed wavenumber are two-dimensional flow induced surface instabilities (see [3]). However, there is as yet

no evidence to suggest that the same is true for viscous flows over compliant surfaces. Recent studies, see [14], [15] and [5] have, in fact, suggested that compliant walls are much more susceptible to three-dimensional instabilities than rigid walls. In [5] it was shown that for compliant walls with good transition delaying properties, obliquely propagating three-dimensional waves are likely to be more unstable than the two-dimensional waves. Indeed YEO, [16], showed that the stability of two-dimensional boundary layers is characterized by a strong degree of three-dimensionality and there are no a priori grounds to assume that the most unstable modes will be two-dimensional.

Studies on two- and three-dimensional disturbances in a two-dimensional boundary layer have also been carried out in [4]. In this study, the triple-deck theory is used to investigate the evolution of the disturbances over isotropic and anisotropic compliant walls. The study showed that viscous effects have a much more profound influence on disturbances in the boundary layers over anisotropic compliant walls in comparison with isotropic compliant walls. However, the study does not give any indication of how the compliance parameters (such as mass density, visco-elastic damping, etc.) affect the behaviour of the disturbances over each class of compliant walls. The study by JOSLIN and others, [8], suggested that properly designed compliant walls can stabilize three-dimensional wave modes despite the fact that these modes may be growing faster than two-dimensional modes.

Detailed studies of three-dimensional wave modes in flows over compliant walls have also been made in [14] and [16]. The study in [16] provides a summary of the three-dimensional results in [14] with additional new results. Comparisons with two-dimensional wave modes are made for the flow over a two-dimensional boundary layer. The effects of wall stiffness and material damping on each class of waves is carefully analyzed. It is found that for sufficiently compliant walls, increasing wall stiffness tends to promote the dominance of three-dimensional TSI modes over two-dimensional modes. Material damping was also shown to play an important role in determining the relative dominance of the two- and three-dimensional modes.

In [12] the effect of thermal buoyancy on the linear stability of three-dimensional waves was considered. It was found that the effect of three-dimensional modes is more significant than that of two-dimensional modes when the wavenumber is varied against the tension parameter, the spring stiffness and the flexural rigidity of the flexible surface. In this paper the effects of three-dimensional disturbances on the stability of two-dimensional channel flow with one compliant surface in the absence of thermal buoyancy are studied. The study extends the analysis made in [6] to three-dimensional disturbances.

2. Mathematical formulation

2.1. The equations of motion

Consider the flow of an incompressible fluid in a channel of infinite extent and with one compliant surface. The equations governing the motion of three-dimensional disturbances spreading within the channel can be expressed in non-dimensional form as:

$$(2.1) \quad \frac{\partial u}{\partial x} + \frac{\partial v}{\partial y} + \frac{\partial w}{\partial z} = 0,$$

$$(2.2) \quad \frac{Du}{Dt} = -\frac{\partial p}{\partial x} + \frac{1}{R} \left(\frac{\partial^2 u}{\partial x^2} + \frac{\partial^2 u}{\partial y^2} + \frac{\partial^2 u}{\partial z^2} \right),$$

$$(2.3) \quad \frac{Dv}{Dt} = -\frac{\partial p}{\partial y} + \frac{1}{R} \left(\frac{\partial^2 v}{\partial x^2} + \frac{\partial^2 v}{\partial y^2} + \frac{\partial^2 v}{\partial z^2} \right),$$

$$(2.4) \quad \frac{Dw}{Dt} = -\frac{\partial p}{\partial z} + \frac{1}{R} \left(\frac{\partial^2 w}{\partial x^2} + \frac{\partial^2 w}{\partial y^2} + \frac{\partial^2 w}{\partial z^2} \right),$$

where p is the pressure, R is the Reynolds number, x , y and z are respectively, the streamwise, the normal and spanwise coordinates, u is the velocity component in the streamwise direction with v and w being respectively the velocity components in the y and z directions and t is time. Equations (2.1)–(2.4) have been non-dimensionalised by setting

$$(x', y', z') = L(x, y, z), \quad (u', v', w') = U_B(u, v, w) \quad \text{and} \quad R = U_B L / \nu_*,$$

where the primes denote dimensional quantities, L is the undisturbed channel width, U_B is the channel centreline speed and ν_* is the coefficient of kinematic viscosity of the fluid.

2.2. The flexible wall equations

In this study we restrict the motion of the compliant surface to only vertical displacements. At the upper rigid channel wall, the fluid motion satisfies the no-slip constraint

$$u = v = w = 0, \quad \text{at} \quad y = 1,$$

while at the lower flexible surface the fluid motion is governed by

$$u = w = 0, \quad v = \frac{\partial \eta}{\partial t} \quad \text{at} \quad y = \eta(x, z, t).$$

The surface displacement $\eta(x, z, t)$ satisfies the dynamic condition (see for example, [11])

$$(2.5) \quad \nabla p = \frac{T}{R^2} \left(\frac{\partial^2 \eta}{\partial x^2} + \frac{\partial^2 \eta}{\partial z^2} \right) - M \frac{\partial^2 \eta}{\partial t^2} - \frac{d}{R} \frac{\partial \eta}{\partial t} \\ - \frac{B}{R^2} \left(\frac{\partial^4 \eta}{\partial x^4} + 2 \frac{\partial^4 \eta}{\partial x^2 \partial z^2} + \frac{\partial^4 \eta}{\partial z^4} \right) - \frac{\kappa}{R^2} \eta.$$

The non-dimensional physical parameters M, d, B, T and κ are respectively the mass density per unit length, the damping, the flexural rigidity of the plate, the tension and the spring stiffness while ∇p is the change in the mechanical fluid pressure. Equation (2.5) has been non-dimensionalised using the fluid density ρ_* , the density of the plate material ρ_m , the channel width L , the centre-line velocity U_B and the viscosity μ_* where

$$(x, z, t) = \frac{1}{L} (x', z', U_B t'), \quad \eta = \frac{\eta'}{L}, \quad \nabla p = \frac{\nabla p'}{\rho_* U_B^2}, \quad T = \frac{T' \rho_* L}{\mu_*^2}, \\ \kappa = \frac{\kappa' L^3 \rho_*}{\mu_*^2}, \quad M = \frac{\rho_m b'}{\rho_* L}, \quad d = \frac{d' L}{\mu_*}, \quad B = B' \rho_* \mu_*^2 L.$$

The asymptotic structure for the upper branch stability of channel flows is now well-known, see for example [13]. This enables us, for large Reynolds number, to define a small parameter $\epsilon = R^{-1/11}$ and introduce scaled flow variables ξ, X, Z and T defined by:

$$X = \epsilon^3 x, \quad Z = \epsilon^3 z, \quad T = \epsilon^5 t, \quad \xi = \epsilon(\alpha_0 x + \beta_0 z - \epsilon^2 \alpha_0 c_0 t),$$

where α_0 and β_0 are respectively the scaled real wavenumbers in the streamwise and spanwise directions and c_0 is the scaled phase velocity of the waves. The frequency of the disturbances ω_0 and the oblique wavenumber γ_0 are defined by $\omega_0 = \alpha_0 c_0$ and $\gamma_0^2 = \alpha_0^2 + \beta_0^2$ respectively. In terms of the slow variables, the derivatives in Eqs. (2.1)–(2.4) become

$$(2.6) \quad \frac{\partial}{\partial t} \rightarrow -\epsilon^3 \alpha_0 c_0 \frac{\partial}{\partial \xi} + \epsilon^5 \frac{\partial}{\partial T}, \\ \frac{\partial}{\partial x} \rightarrow \epsilon \alpha_0 \frac{\partial}{\partial \xi} + \epsilon^3 \frac{\partial}{\partial X}, \quad \frac{\partial}{\partial z} \rightarrow \epsilon \beta_0 \frac{\partial}{\partial \xi} + \epsilon^3 \frac{\partial}{\partial Z},$$

so that Eqs. (2.1)–(2.4) can now be written in the form:

$$\begin{aligned}
 & \left(\alpha_0 \epsilon \frac{\partial}{\partial \xi} + \epsilon^3 \frac{\partial}{\partial X} \right) u + \frac{\partial v}{\partial Y} + \left(\epsilon \beta_0 \frac{\partial}{\partial \xi} + \epsilon^3 \frac{\partial}{\partial Z} \right) w = 0, \\
 & \epsilon^3 \left(-\alpha_0 c_0 \frac{\partial}{\partial \xi} + \epsilon^2 \frac{\partial}{\partial T} \right) u + \epsilon u \left(\alpha_0 \frac{\partial}{\partial \xi} + \epsilon^2 \frac{\partial}{\partial X} \right) u + v \frac{\partial u}{\partial Y} \\
 & + \epsilon w \left(\beta_0 \frac{\partial}{\partial \xi} + \epsilon^2 \frac{\partial}{\partial Z} \right) u = -\epsilon \left(\alpha_0 \frac{\partial}{\partial \xi} + \epsilon^2 \frac{\partial}{\partial X} \right) p + \epsilon^{11} \left(\frac{\partial^2 u}{\partial x^2} + \frac{\partial^2 u}{\partial y^2} + \frac{\partial^2 u}{\partial z^2} \right), \\
 (2.7) \quad & \epsilon^3 \left(-\alpha_0 c_0 \frac{\partial}{\partial \xi} + \epsilon^2 \frac{\partial}{\partial T} \right) v + \epsilon u \left(\alpha_0 \frac{\partial}{\partial \xi} + \epsilon^2 \frac{\partial}{\partial X} \right) v + v \frac{\partial v}{\partial Y} \\
 & + \epsilon w \left(\beta_0 \frac{\partial}{\partial \xi} + \epsilon^2 \frac{\partial}{\partial Z} \right) v = -\frac{\partial p}{\partial Y} + \epsilon^{11} \left(\frac{\partial^2 v}{\partial x^2} + \frac{\partial^2 v}{\partial y^2} + \frac{\partial^2 v}{\partial z^2} \right), \\
 & \epsilon^3 \left(-\alpha_0 c_0 \frac{\partial}{\partial \xi} + \epsilon^2 \frac{\partial}{\partial T} \right) w + \epsilon u \left(\alpha_0 \frac{\partial}{\partial \xi} + \epsilon^2 \frac{\partial}{\partial X} \right) w + v \frac{\partial w}{\partial Y} \\
 & + \epsilon w \left(\beta_0 \frac{\partial}{\partial \xi} + \epsilon^2 \frac{\partial}{\partial Z} \right) w = -\epsilon \left(\beta_0 \frac{\partial}{\partial \xi} + \epsilon^2 \frac{\partial}{\partial Z} \right) p + \epsilon^{11} \left(\frac{\partial^2 w}{\partial x^2} + \frac{\partial^2 w}{\partial y^2} + \frac{\partial^2 w}{\partial z^2} \right).
 \end{aligned}$$

In this study we consider a three-dimensional disturbance wave of amplitude $O(\delta)$ where this $\delta \ll 1$ and depends on the Reynolds number. This study focuses only on linear disturbances and from [7], it is well known that the first significant departure from linear theory occurs only when $\delta \sim O(R^{-14/33})$.

2.3. The flow regions

The flow region is a multi-deck asymptotic structure identical to that in [6] which consists of seven distinct regions for each of the lower and upper halves of the channel including the shared main inviscid region $R1$ in Fig. 1. Our focus is on the upper-branch stability so that the viscous wall layer (Stokes layer) and the critical layer are distinct. Following [10, 12] and other earlier authors, our solution technique consists of deriving asymptotic expansions of the solution in various regions followed by appropriate matching at the subdomain boundaries. We first consider the solution in the core region $R1$. Let $(U_B, 0, 0, p_B)$ be the steady state laminar flow and superimpose a small perturbation so that the perturbed total flow takes the form

$$\begin{aligned}
 (2.8) \quad & (u, v, w) = (U_B, 0, 0) + \delta(\tilde{u}_0, \epsilon \tilde{v}_0, \epsilon^2 \tilde{w}_0) + \delta \epsilon^2(\tilde{u}_1, \epsilon \tilde{v}_1, \epsilon^2 \tilde{w}_1) + \dots, \\
 & p = p_B + \delta \epsilon^2 \tilde{p}_0 + \delta \epsilon^4 \tilde{p}_1 + \dots,
 \end{aligned}$$

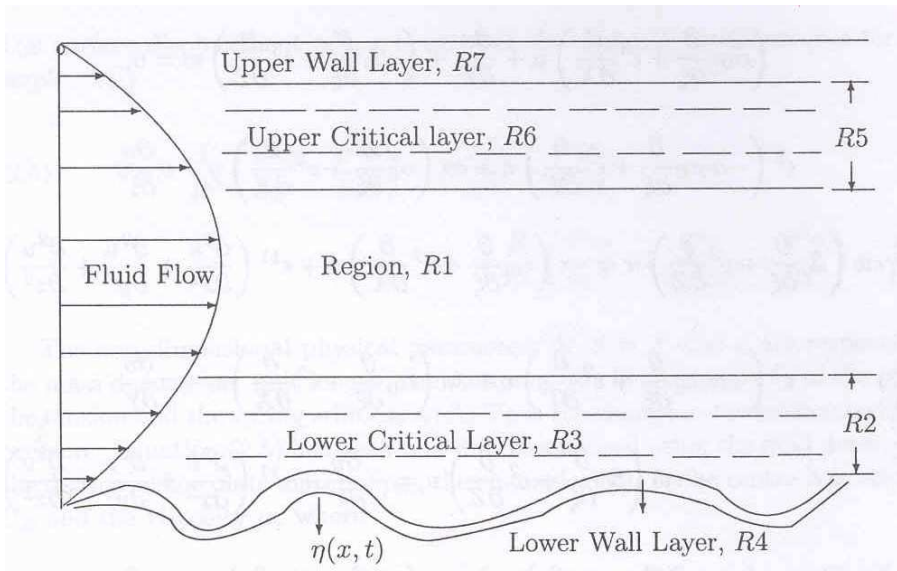


FIG. 1. Schematic diagram of the channel cross-section illustrating the multi-deck fluid flow structure. The lower flexible surface can be modelled by an elastic plate or a continuous springy elastic foundation.

where \tilde{u}_i , \tilde{v}_i , \tilde{w}_i and \tilde{p}_i are functions of the boundary layer variables Y , ξ , X , Z and T . The expansions (2.8) are now substituted into Eqs. (2.7). If we equate the leading order terms, a system of differential equations is obtained. These equations give the leading order solutions

$$(2.9) \quad \tilde{u}_0 = AU_{By}, \quad \tilde{v}_0 = -\alpha_0 A_\xi U_B, \quad \tilde{w}_{0\xi} = -\frac{\beta_0 \tilde{p}_{0\xi}}{\alpha_0 U_B},$$

where $A = \bar{A}(X, Z, T)e^{i\xi} + c.c$ is an unknown displacement function and $c.c$ denotes the complex conjugate. Additionally, the pressure is an integral of the basic flow and an unknown contribution from the lower flexible surface given by

$$(2.10) \quad \tilde{p}_0 = P_0 + \alpha_0^2 A_{\xi\xi} \int_0^y U_B^2 ds,$$

where $P_0 = \bar{P}_0(X, Z, T)e^{i\xi} + c.c$ is the unknown pressure at the lower surface.

At the next order of perturbation quantities, the governing equations give the solutions for the normal velocity component and the pressure as, respectively,

$$(2.11) \quad \tilde{v}_1 = U_B \frac{\gamma_0}{\alpha_0} \int_{1/2}^y \frac{\tilde{p}_{0\xi}}{U_B^2} ds + \alpha_0 c_0 A_\xi - \alpha_0 A_{1\xi} U_B,$$

$$\begin{aligned}
 (2.11) \quad \underset{[\text{cont.}]}{\tilde{p}_1} &= P_1 + \gamma_0^2 \int_0^y U_B^2 \left(\int_{1/2}^y \frac{\tilde{p}_0}{U_B^2} ds_1 \right) ds + 2\alpha_0^2 c_0 A \int_0^y U_B ds \\
 &\quad - \alpha_0 (\alpha_0 A_{1\xi\xi} - A_{X\xi}) \int_0^y U_B^2 ds,
 \end{aligned}$$

where the additional displacement A_1 and the pressure P_1 are unknown functions of X, Z and T . In region $R2$, the appropriate scaled transverse coordinate is $y = \epsilon^2 \bar{Y}$ with $\bar{Y} \sim 0(1)$. The solutions found in region $R1$ imply that the local perturbations take the form

$$\begin{aligned}
 (2.12) \quad u &= \lambda_1 \epsilon^2 \bar{Y} + \lambda_2 \epsilon^4 \bar{Y}^2 + \dots + \delta(\bar{u}_0 + \epsilon^2 \bar{u}_1) + \dots, \\
 (v, w, p) &= (0, 0, p_B) + \delta(\epsilon^3 \bar{v}_0, \bar{w}_0, \epsilon^2 \bar{p}_0) + \delta \epsilon^2 (\epsilon^3 \bar{v}_1, \bar{w}_1, \epsilon^2 \bar{p}_1) + \dots,
 \end{aligned}$$

where

$$\lambda_1 = \frac{dU_B}{dy}, \quad 2\lambda_2 = \frac{d^2U_B}{dy^2} \quad \text{at } y = 0.$$

Substituting the expansions into the equations of motion and solving the resulting differential equations gives the following solutions:

$$\begin{aligned}
 (2.13) \quad \bar{u}_0 &= \lambda_1 A + \frac{\beta_0^2 \bar{p}_0}{\alpha_0^2 (\lambda_1 \bar{Y} - c_0)}, & \bar{v}_0 &= -\gamma_0^2 \frac{\bar{p}_0 \xi}{\lambda_1 \alpha_0} - \alpha_0 A_\xi (\lambda_1 \bar{Y} - c_0), \\
 \bar{w}_0 &= -\frac{\beta_0 \bar{p}_0}{\alpha_0 (\lambda_1 \bar{Y} - c_0)}, & \bar{p}_0 &= P_0(X, Z, T).
 \end{aligned}$$

It is worth noting here that in this three-dimensional analysis, \bar{u}_0 and \bar{w}_0 exhibit a pole-type singularity when $\zeta = \bar{Y} - c_0/\lambda_1 \rightarrow 0$, unlike the corresponding two-dimensional problem where such a singularity is not found in \bar{u}_0 .

The second-order velocity component \bar{v}_1 is given by

$$\begin{aligned}
 (2.14) \quad \bar{v}_1 &= -\frac{\gamma_0^2 \bar{p}_1 \xi}{\lambda_1 \alpha_0} - \frac{2\beta_0 \bar{p}_0 Z}{\lambda_1 \alpha_0} + \left(\frac{\beta_0^2}{\alpha_0^2} - 1 \right) \frac{\bar{p}_0 X}{\lambda_1} - (A_T + c_0 A_X) \\
 &\quad - i\alpha_0 \frac{\lambda_2}{\lambda_1} A \left(\zeta^2 + 2\frac{c_0}{\lambda_1} \zeta \{ \ln |\zeta| + \phi^\pm \} - \frac{c_0^2}{\lambda_1^2} \right) \\
 &\quad - 2i\alpha_0 c_0 \frac{\lambda_2}{\lambda_1} \eta_0 \left[\zeta \{ \ln |\zeta| + \phi^\pm \} - \frac{c_0}{\lambda_1} \right] - i\bar{A}_1 \alpha_0 \lambda_1 \zeta,
 \end{aligned}$$

where \bar{A}_1 is an unknown function of X, Z, T and $\bar{p}_1 = P_1 e^{i\xi}$. This solution contains terms that are irregular when $\zeta = 0$, called the critical level. A thin

region, the critical layer, is thus introduced on either side of this level and the terms ϕ^\pm are introduced to smooth the solution across this critical layer (the + sign refers to positive ζ and the - refers to negative ζ). In the linear theory it is now well established that $\phi^+ - \phi^- = i\pi$. Similar terms can be found in [12] and in the references therein.

2.4. The compliant wall conditions

The equation for the wall motion, (2.5), is rewritten in the form

$$(2.15) \quad \nabla p = p' = \bar{T}(\eta_{xx} + \eta_{zz}) - M_s \epsilon^{-4} \eta_{tt} - \bar{d} \epsilon \eta_t \\ - B_s \epsilon^2 (\eta_{xxxx} + 2\eta_{xxzz} + \eta_{zzzz}) - \kappa_s \epsilon^2 \eta,$$

where the constants \bar{T} , M_s , B_s , \bar{d} and κ_s are related to the original constants in Eq. (2.5) by

$$(2.16) \quad \bar{T} = \frac{T}{R^2}, \quad M_s = M \epsilon^4, \quad B_s = \frac{B}{\epsilon^2 R^2}, \quad \bar{d} = \frac{d}{\epsilon R}, \quad \kappa_s = \frac{\kappa}{\epsilon^2 R^2}.$$

This choice of scalings is motivated by equations (2.6) and ensures the retention of the influence of wall parameters in the eigenvalue problem. In particular, it enables the scaled parameters to appear as $O(1)$ constants in the eigenvalue problem.

The fluctuating pressure at the wall, p' and the surface displacement are expanded in the form

$$p' = \delta(\epsilon^2 \hat{p}_0 + \epsilon^4 \hat{p}_1) + \dots \quad \text{and} \quad \eta = \delta(\eta_0 + \epsilon^2 \eta_1) + \dots.$$

Setting $\eta_i = \hat{\eta}_i(X, Z, T) e^{i\xi} + c.c.$ (for $i = 0, 1, \dots$) and matching the solutions in regions $R1$ and $R2$ shows that the vertical displacement of the lower wall is related to the amplitude of the disturbances by

$$(2.17) \quad \eta_0 = \frac{\alpha_0^2 c_0 \lambda_1 A}{s_0 \gamma_0^2 - \alpha_0^2 c_0 \lambda_1} \quad \text{where} \quad s_0 = -\gamma_0^2 T_0 + M_s \alpha_0^2 c_0^2 - \gamma_0^4 B_s - \kappa_s.$$

At the next order we obtain

$$(2.18) \quad \hat{p}_1 = \bar{P}_1 = s_0 \eta_1 + 2i\bar{T}(\alpha_0 \eta_{0X} + \beta_0 \eta_{0Z}) + i\bar{d} \alpha_0 c_0 \eta_0 \\ + 2iM_s \alpha_0 c_0 \eta_{0T} + 4iB_s(\alpha_0^3 \eta_{0X} + \beta_0^3 \eta_{0Z}).$$

In addition to the analysis for the inviscid regions $R1$ and $R2$ and the wall conditions considered above, it is also necessary to consider the motion of the fluid in the region $R4$, the Stokes layer, adjacent to the moving wall surface.

In particular, the solutions in region $R2$ do not satisfy the no-slip conditions at the wall and it is therefore necessary to introduce this viscous layer with $y = \eta(x, z, t) + \epsilon^4 Y$ where Y is the $0(1)$ coordinate and $U_B \sim \epsilon^4 \lambda_1 Y + \dots$ as $y \rightarrow 0$. The total flow takes the form

$$\begin{aligned} u &= U_B + \delta \hat{u}_0 + \dots, & v &= -\epsilon^3 \delta \alpha_0 c_0 \eta_\xi + \delta \epsilon^5 \hat{v}_0 + \dots, \\ w &= \delta \hat{w}_0 + \epsilon^2 \delta \hat{w}_1 + \dots, & p &= p_B + \delta \epsilon^2 \hat{p}_0 + \dots. \end{aligned}$$

The leading order equations which govern the Stokes layer flow are a linear system of partial differential equations similar to those derived in [2] but with the streamwise momentum equation slightly modified by the compliance of the lower surface. These are

$$(2.19) \quad i\alpha_0 \hat{u}_0 + \hat{v}_{0Y} + i\beta_0 \hat{w}_0 = 0, \quad -i\alpha_0 c_0 (\hat{u}_0 + \lambda_1 \eta_0) = -i\alpha_0 \hat{p}_0 + \hat{u}_{0YY},$$

$$(2.20) \quad \hat{p}_{0Y} = 0, \quad -i\alpha_0 c_0 \hat{w}_0 = -i\beta_0 \hat{p}_0 + \hat{w}_{0YY}.$$

The boundary conditions are obtained by requiring a matching of the solutions to the above equations with the flow in region $R2$ and that there should be no slip at the lower wall, giving

$$(2.21) \quad \hat{u}_0 \sim \lambda_1 A - \frac{\beta_0^2}{\alpha_0 c_0} \bar{p}_0, \quad \hat{w}_0 \sim \frac{\beta_0}{\alpha_0 c_0} \bar{p}_0 \quad \text{as} \quad Y \rightarrow \infty,$$

$$(2.22) \quad \hat{u}_0 = -\lambda_1 \eta_0, \quad \hat{v}_0 = \hat{w}_0 = 0 \quad \text{at} \quad Y = 0.$$

The solutions to the above system of equations are

$$(2.23) \quad \hat{u}_0 = \frac{\hat{p}_0}{c_0} \left\{ 1 - \exp(-mY) \right\} - \lambda_1 \eta, \quad \hat{w}_0 = \frac{\beta_0 \hat{p}_0}{\alpha_0 c_0} \left\{ 1 - \exp(-mY) \right\},$$

where $m = (\alpha_0 c_0)^{1/2} e^{-i\pi/4}$. The solution for \hat{v}_0 becomes

$$(2.24) \quad \hat{v}_0 = -i\gamma_0^2 \frac{\hat{p}_0}{\alpha_0 c_0} \left(Y + \frac{\exp(-mY)}{m} - \frac{1}{m} \right) + i\alpha_0 \lambda_1 Y \eta.$$

In deriving the amplitude equation, we are interested in the finite part of \hat{v}_0 as $Y \rightarrow \infty$. This is obtained from (2.24), and is given by

$$(2.25) \quad \hat{v}_{0f} = \frac{i\gamma_0^2 \hat{p}_0}{m c_0 \alpha_0}.$$

Having considered the solution of the problem in the lower half of the channel, it is now necessary to consider the solutions in the upper half, namely regions $R5$ to $R7$ in Fig. 1. However, except for the boundary conditions, stating that the

normal velocity vanishes identically at the top wall, the derivation and analysis of the perturbed flow is similar to that already outlined above for regions $R2$ to $R4$. As such, we omit most of the details and give below the main perturbation solutions for the regions $R5$ to $R7$ close to the top rigid wall. We use the notation \tilde{u}_0 , \tilde{v}_0 , \tilde{w}_0 and \tilde{p}_0 to represent the leading order streamwise, normal, spanwise and pressure perturbations at the upper end of the channel.

In region $R5$, which contains the upper critical layer, the leading order solutions for the perturbation velocity and pressure quantities are found to be

$$(2.26) \quad \tilde{u}_0 = \hat{\lambda}_1 A + \frac{\beta_0^2}{\alpha_0^2} \frac{\tilde{p}_0}{(\hat{\lambda}_1 \tilde{Y} - c_0)}, \quad \tilde{v}_0 = -i\alpha_0 A \tilde{Y},$$

and

$$(2.27) \quad \tilde{w}_0 = -\frac{\beta_0}{\alpha_0} \frac{\tilde{p}_0}{(\hat{\lambda}_1 \tilde{Y} - c_0)}, \quad \tilde{p}_0 = \frac{\alpha_0^2 c_0 \hat{\lambda}_1}{\gamma_0^2} A,$$

where $\hat{\lambda}_1 = U_{By}|_{y=1}$ and $2\hat{\lambda}_2 = U_{Byy}|_{y=1}$ and \tilde{Y} is the $O(1)$ normal coordinate. The leading order streamwise and spanwise velocity components are found, as expected, to exhibit a pole-type singularity in the vicinity of the critical layer.

The normal velocity and pressure components of second order have the solutions

$$(2.28) \quad \begin{aligned} \tilde{v}_1 = & -\frac{i\gamma_0^2}{\hat{\lambda}_1 \alpha_0} \tilde{p}_1 - \frac{1}{\hat{\lambda}_1} \left(1 - \frac{\beta_0^2}{\alpha_0^2} \right) \tilde{p}_{0X} - \frac{2\beta_0}{\alpha_0 \hat{\lambda}_1} \tilde{p}_{0Z} - (A_T + c_0 A_X) \\ & - i\alpha_0 \hat{\lambda}_2 A \left(\tilde{\xi}^2 + 2\frac{c_0}{\hat{\lambda}_1} \tilde{\xi} [\ln |\tilde{\xi}| + \tilde{\phi}^\pm] - \frac{c_0^2}{\hat{\lambda}_1} \right) - i\tilde{A}_1 q \alpha_0 \tilde{\lambda}_1 \tilde{\xi}, \\ \tilde{p}_1 = & \tilde{p}_1(X, Z, T), \end{aligned}$$

where $\tilde{\xi} = \tilde{Y} - c_0/\hat{\lambda}_1$ and the terms $\tilde{\phi}^\pm$ represent the phase jump across the upper critical layer. From the analysis of the Stokes layer near the upper rigid wall, the displacement condition on \tilde{v}_1 is found to be

$$(2.29) \quad \tilde{v}_1(\tilde{Y} = 0) = -i \frac{\gamma_0^2 \tilde{p}_0}{c_0 m \alpha_0}.$$

3. Linear stability neutral curve results

The analysis of the results obtained in the previous sections is similar to that of the two-dimensional disturbance waves given in [6]. In particular, matching the leading order solutions across the regions leads to the dispersion relation for the three-dimensional disturbances:

$$(3.1) \quad \frac{\alpha_0^2 c_0^2 \lambda_1^2}{s_0 \gamma_0^2 - \alpha_0^2 c_0 \lambda_1} = \gamma_0^2 I_0 + c_0 (\hat{\lambda}_1 - \lambda_1).$$

We note that if $\beta_0 = 0$ then $\gamma_0 = \alpha_0$ and the dispersion relation is just that for the two-dimensional waves in [6]. The second expression obtained by eliminating $P_1, \bar{A}_1, \eta_1, \tilde{A}_1, \tilde{p}_0$ and \tilde{p}_1 from the solutions outside the critical layer is

$$\begin{aligned}
 (3.2) \quad & iA(c_0D_6 - \lambda_1D_7) + \frac{i\alpha_0\lambda_1^2s_0A}{m(s_0a_0 - c_0\lambda_1)} \\
 & + \frac{c_0\lambda_1\gamma_0^2}{\alpha_0s_0a_0} \left[-2\bar{T}(i\alpha_0\eta_{0X} + i\beta_0\eta_{0Z}) - \bar{d}\alpha_0c_0\eta_0 \right] \\
 & + \frac{c_0\lambda_1\gamma_0^2}{\alpha_0s_0\alpha_0} \left[-2M_s\alpha_0c_0\eta_{0T} - 4B_s(\alpha_0^3\eta_{0X} + \beta_0^3\eta_{0Z}) \right] + \lambda_1\eta_{0T} - i\alpha_0c_0\lambda_1A_{11} \\
 & = 2i\alpha_0c_0^2\frac{\lambda_2}{\lambda_1}(A + \eta_0)(\phi^+ - \phi^-) - \frac{a_1c_0\lambda_1s_0}{s_0a_0 - c_0\lambda_1}A_Z - \frac{a_2c_0\lambda_1s_0}{s_0a_0 - c_0\lambda_1}A_X \\
 & - \left(1 - \frac{c_0\lambda_1}{s_0a_0}\right) \left[2i\alpha_0c_0^2\frac{\hat{\lambda}_2}{\hat{\lambda}_1}(\tilde{\phi}^+ - \tilde{\phi}^-)A + \gamma_0^2A_XI_0 + i\alpha_0(\gamma_0^2I_0 + c_0\hat{\lambda}_1)A_{11} \right. \\
 & \quad \left. - \frac{a_2c_0\hat{\lambda}_1}{a_0}A_X - \lambda_1(A_T - c_0A_X) - 2\frac{\alpha_0c_0\hat{\lambda}_1\beta_0}{\gamma_0^2}A_Z - \hat{\lambda}_1(A_T + c_0A_X) \right. \\
 & \quad \left. - iD_9A + \frac{i\alpha_0^3c_0\hat{\lambda}_1}{c_0m\gamma_0^2}A \right],
 \end{aligned}$$

where A_{11} represents the $e^{i\xi}$ component of A_1 . Here $a_0 = \alpha_0^{-2}\gamma_0^2$, $a_1 = 2\alpha_0^{-1}\beta_0$, $a_2 = 2 - a_0$ and the real constants D_6, D_7, D_9 are given in the Appendix.

The expression (3.2) can further be simplified by noting that the dispersion relation implies that the coefficient of A_{11} is zero. We also observe a strong dependence of the evolution equation on the properties of the critical layer through the jumps $(\phi^+ - \phi^-)$ and $(\tilde{\phi}^+ - \tilde{\phi}^-)$.

In order to make a systematic study of the above equation, we restrict ourselves to the neutral case and use the standard linear jump conditions $\phi^+ - \phi^- = i\pi$ and $\tilde{\phi}^+ - \tilde{\phi}^- = -i\pi$. The real part of Eq. (3.2) gives

$$\begin{aligned}
 (3.3) \quad & \frac{2\alpha_0c_0^2\lambda_2s_0a_0\pi}{\lambda_1(s_0a_0 - c_0\lambda_1)} + \frac{2\alpha_0c_0^2\lambda_2}{\lambda_1} \frac{(s_0a_0 - c_0\lambda_1)}{s_0a_0} = -\frac{c_0^3\gamma_0^2\lambda_1^2d_{1r}}{s_0a_0(s_0a_0 - c_0\lambda_1)} \\
 & - \frac{\alpha_0\lambda_1^2s_0}{\sqrt{2}\bar{m}(s_0a_0 - c_0\lambda_1)} - \frac{\alpha_0^3\lambda_1^2(s_0a_0 - c_0\lambda_1)}{\sqrt{2}\bar{m}s_0a_0\gamma_0^2},
 \end{aligned}$$

where d_{1r} is the real part of \bar{d} . It can be seen that the characteristic equations form two equations in three unknown variables, namely, α_0, β_0 and c_0 . In general, in order to be able to determine all the eigenvalues, an additional criterion

or relationship must be supplemented. However, for our purposes, attention is focused on oblique waves which grow only in the direction of propagation. In this case γ_0 becomes the sole eigenvalue with $\alpha_0 = \gamma_0 \cos \theta$ and $\beta_0 = \gamma_0 \sin \theta$, where θ is the angle of propagation of the disturbance. With these modifications, the characteristic eigenvalue relationships become characteristic equations for the eigenvalues α_0 and c_0 .

4. Analysis of limiting cases

In order to obtain an intuitive understanding of the effects of the flexible surface material parameters on the fluid flow, we consider a number of limiting cases when some of the parameters are either large or small. An exhaustive parametric study would be mathematically intractable on account of the large number of physical parameters present.

The cases singled out here have been chosen so that $s_0 = -\gamma_0^2 T_0 + M_s \alpha_0^2 c_0^2 - \gamma_0^4 B_s - \kappa_s$ reduces to a simple form that would allow for a detailed examination of Eq. (3.3).

(i) $T_0 = B_s = M_s = 0$, d_{1r} finite and $k_s \rightarrow \infty$.

Physically, with the surface parameters having these values, the motion of the wall surface would effectively be governed by Hooke's law. If $k_s \rightarrow \pm\infty$ (which implies increasing rigidity of the compliant surface) then $s_0 \rightarrow \pm\infty$ and α_0 , c_0 approach the three-dimensional rigid-wall values:

$$(4.1) \quad \alpha_{0r} = \lambda_1 \left(\frac{4 \cos^{14} \theta}{\lambda_2^2 \pi^2 I_0^5} \right)^{1/11}, \quad c_{0r} = \frac{\alpha_0^2 I_0}{2 \lambda_1 \cos^2 \theta}.$$

The equivalent two-dimensional values are given by Eq. (5.2) of [6].

(ii) $d_{1r} \rightarrow \infty$.

In this limit both α_0 and c_0 become large, indicating a possible destabilization of the flow. As in the corresponding two-dimensional problem, the precise limiting case depends on the values of the other physical parameters, namely, T_0 , M_s and B_s . Thus, for example, when $T_0 = M_s = B_s = 0$ and k_s is finite, we obtain

$$(4.2) \quad c_0 = \frac{\alpha_0^2 I_0}{\lambda_1 \cos^2 \theta}, \quad \alpha_0 = \frac{\lambda_1^2 d_{1r}}{2 \lambda_2 \pi I_0}.$$

If $M_s = 0$, $B_s \neq 0$, $T_0 \neq 0$ and $k_s \neq 0$

$$(4.3) \quad c_0 = \frac{\alpha_0^2 I_0}{2 \lambda_2 \cos^2 \theta}, \quad \alpha_0 = \left(\frac{-\lambda_1^2 I_0 d_{1r}}{8 B_s^2 \lambda_2 \pi} \right)^{1/5}.$$

If $M_s \neq 0$, $B_s \neq 0$, $T_0 \neq 0$ and $k_s \neq 0$,

$$(4.4) \quad c_0 = \frac{\alpha_0^2 I_0}{2\lambda_2 \cos^2 \theta}, \quad \alpha_0 = \left(\frac{-2\lambda_1^6 \cos^8 \theta d_{1r}}{M_s^2 \pi \lambda_2 I_0^3} \right)^{1/9}.$$

The above results all indicate the destabilizing nature of viscoelastic damping. However, increasing the mass density M_s and the rigidity B_s may have the effect of counteracting the effects of large damping, as seen from Eqs. (4.3) and (4.4).

5. Neutral stability curves

In this section we present a limited parametric study of the eigenvalue problem (3.3) in order to gain a qualitative and quantitative understanding of how the various surface parameters affect the stability of the three-dimensional disturbances. Figures 2 to 4 show the response of the three-dimensional disturbances to changes in parametric values.

The results show the variation of the neutral wavenumber α_0 against the wall stiffness parameter κ_s , the wall tension T_0 and the damping parameter, d_{1r} . These results are compared with the corresponding two-dimensional results of [6] (which are illustrated by dotted lines).

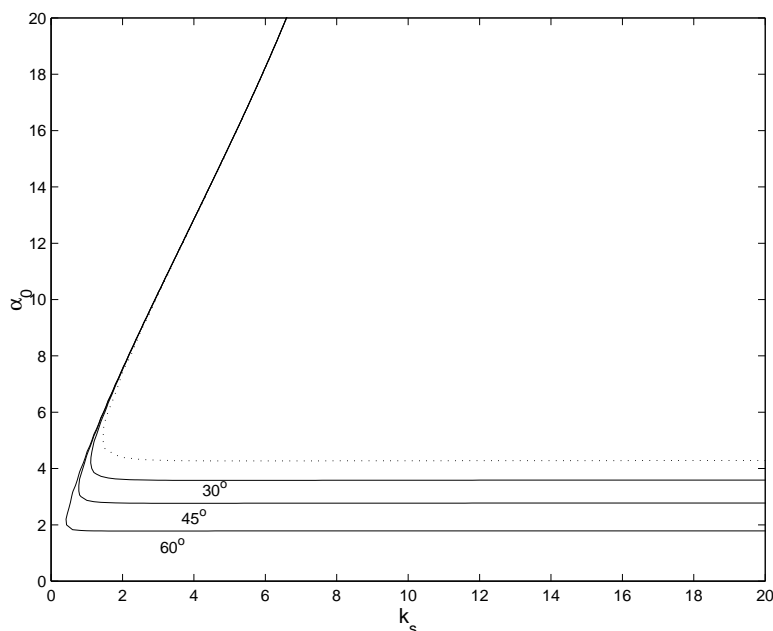


FIG. 2. Plot of the linear neutral wavenumber α_0 versus the scaled spring stiffness parameter k_s with $d_{1r} = 10$ and $T_0 = M_s = B_s = 0$ fixed.

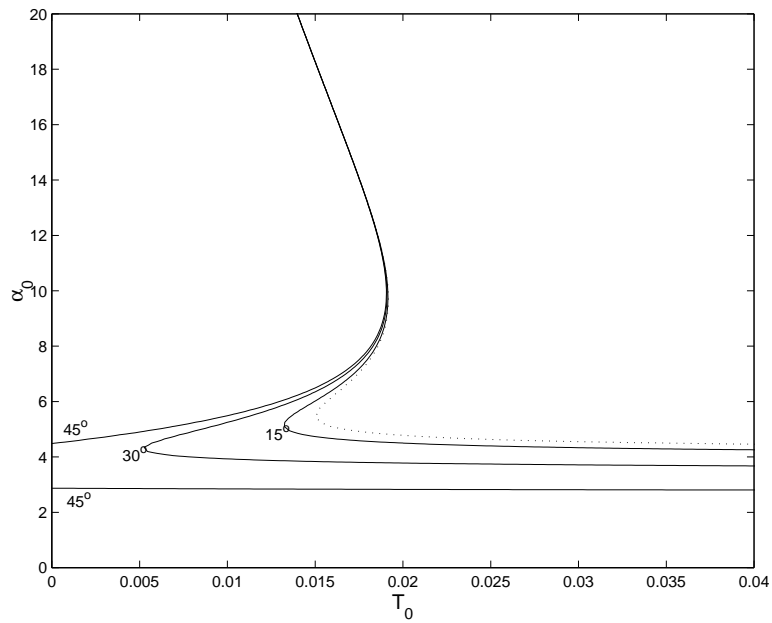


FIG. 3. Plot of the linear neutral wavenumber α_0 against the tension parameter T_0 with other parameters having fixed values: $d_{1r} = 10$, $k_s = 1$ and $M_s = B_s = 0$.

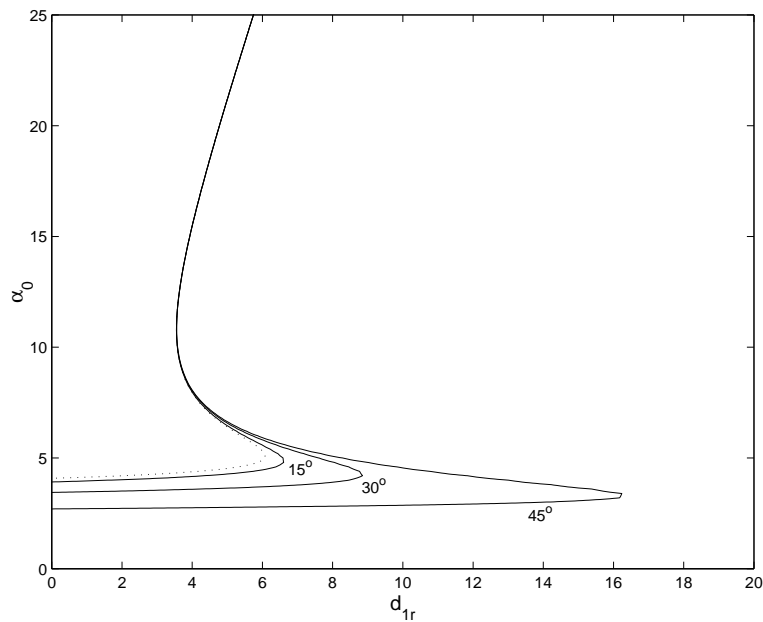


FIG. 4. Plot of the linear neutral wavenumber α_0 against the damping parameter d_{1r} with other wall parameters assuming fixed constant values: $k_s = 1$, $T_0 = 0.001$ and $M_s = B_s = 0$.

Figure 2 shows the variation of the neutral wavenumber α_0 with respect to the wall stiffness parameter k_s for $d_{1r} = 10$, $\theta = 30^\circ, 45^\circ, 60^\circ$ with all other parameters set to zero. It can be seen that as k_s becomes large, the wavenumber α_0 tends to the rigid wall limit which depends on the degree of three-dimensionality of the disturbances, as characterized by the angle θ . This has been predicted in the analysis of the limiting cases, cf. equations (4.1) above. The wavenumbers for the approach to the rigid wall limit are, however, much smaller than those for the corresponding two-dimensional case of [6].

For some finite values of compliant surface parameters T_0 , κ_s and d_{1r} , Figs. 2–4 show that the wavenumbers and consequently, the wave speeds grow without limit. What is of particular interest however is that, in the vicinity of these critical values of compliant parameters, Figs. 3 and 4 appear to suggest that a branch of the three-dimensional disturbances has marginally larger wavenumbers than the corresponding two-dimensional modes, particularly for large values of θ . This appears to support the conclusion in [16] that for a flow over compliant surfaces, two-dimensional modes may not necessarily be the most unstable. A choice of surface parameters may be found that would promote the dominance of three-dimensional modes.

Figure 3 shows the variation of the neutral wavenumber α_0 against the tension parameter T_0 for $\theta = 15^\circ, 30^\circ, 45^\circ$, $k_s = 1$ and $d_{1r} = 10$ with all other parameters set to zero. We note that an increase in the value of θ leads to smaller wavenumbers when $T_0 \rightarrow 0$ and that the rigid wall limit is approached when T_0 becomes large. A similar trend is observed in Fig. 4. However, Fig. 3 shows the existence of a region, $0.01 \leq T_0 \leq 0.018$, where an “upper-branch” of the three-dimensional disturbances may be slightly more dominant than the two-dimensional modes. This effect is particularly strong for large oblique angles θ , that is for strongly three-dimensional wave modes. The same effect is observed in Fig. 2 for $1 \leq \kappa_s \leq 2$ and in Fig. 4 for $6 \leq d_{1r} \leq 8$.

In Fig. 4 we show the variation of the neutral wavenumber against the damping parameter d_{1r} for $k_s = 1, T_0 = 0.001$, $\theta = 15^\circ, 30^\circ$ and 45° with all other parameters set to zero. Again we see that, except for the region $6 \leq d_{1r} \leq 8$, an increase in the three-dimensionality of the perturbations leads to smaller wavenumbers. However, unlike the case when k_s and T_0 were varied, the rigid wall limit is not recovered when d_{1r} becomes large.

In Figs. 5 and 6 we show the variation of the wavenumber α_0 against the angle θ . In particular, Fig. 5 shows the variation of the neutral wavenumber against the angle θ for $d_{1r} = 20$, $k_s = 0.5, 1, 1.5$ and 2 with all the other parameters set equal to zero. The effect is a decrease of the angle θ at which the wavenumbers become progressively larger. Similar curves were obtained when the wavenumber α_0 was plotted against θ keeping k_s and d_{1r} fixed and varying T_0 and B_s , respectively. As in [12], Figs. 5 and 6 show the existence of two distinct modes, the “lower

branch” corresponding to the rigid wall solutions and the “upper branch” which is as a result of wall compliance.

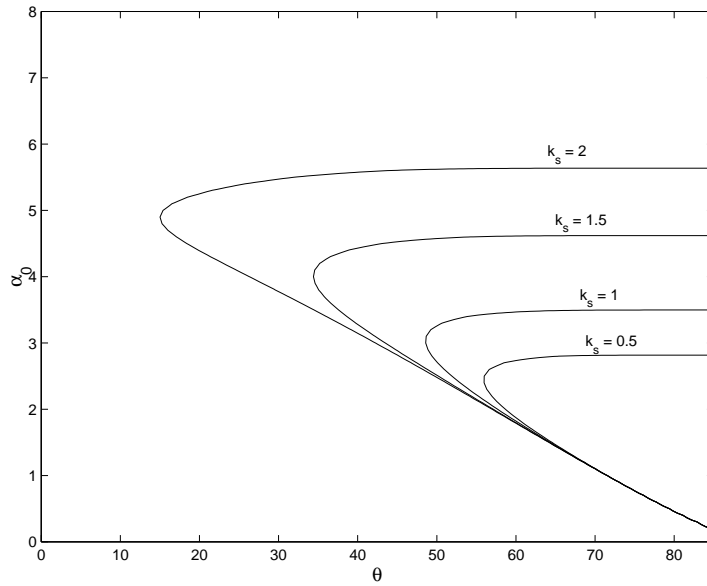


FIG. 5. Plot of the linear neutral wavenumber α_0 against the oblique angle θ for increasing spring stiffness, $k_s = 0.5, 1, 1.5, 2$ and with other wall parameters fixed at $d_{1r} = 20$ and $T_0 = M_s = B_s = 0$.

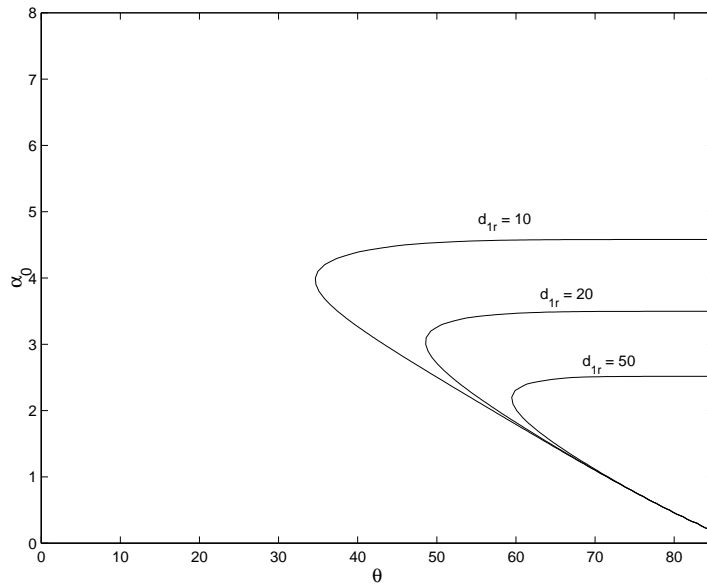


FIG. 6. Plot of the linear neutral wavenumber α_0 against the oblique angle θ for increasing damping, $d_{1r} = 10, 20, 50$ and fixed parameters $k_s = 1$ and $T_0 = M_s = B_s = 0$.

6. Concluding remarks

In this paper we have directly extended the two-dimensional work in [6] to the study of the stability of three-dimensional disturbances in a channel flow with one compliant surface. In order to gain an intuitive understanding of the effects of the compliant surface parameters, we have obtained and analyzed some limiting cases of the linear neutral results. As in the case of two-dimensional disturbances, the effect of damping is seen to be destabilizing. This may, in practice, however be mitigated by the competing effects of other surface parameters.

A limited parametric study was attempted and the results obtained indicate that the three-dimensional disturbances are, in general, more stable than the two-dimensional modes. However, our results also show that a judicious choice of compliant surface parameters could result in three-dimensional modes being more dominant, and consequently more unstable, confirming the conclusion in [16].

Appendix

The integrals I_k and constants D_k appearing in the paper are:

$$\begin{aligned}
 I_0 &= \int_0^1 U_B^2 ds, & I_1 &= \int_0^1 U_B ds, \\
 I_2 &= \int_0^1 U_B \int_{1/2}^{y_1} \frac{1}{U_B^2} ds_1 ds, \\
 I_3 &= \int_0^1 U_B^2 \int_{1/2}^y \frac{1}{U_B^2} \int_0^{y_1} U_B^2 ds_2 ds_1 ds, \\
 I_4 &= \int_{1/2}^0 \left(\frac{1}{U_B^2} - \frac{1}{\lambda_1^2 y^2} + \frac{2\lambda_2}{\lambda_1^3 y} \right) ds, \\
 I_5 &= \int_{1/2}^0 \frac{1}{U_B^2} \int_0^y U_B^2 ds_1 ds, \\
 I_6 &= \int_{1/2}^1 \left(\frac{1}{U_B^2} - \frac{1}{\hat{\lambda}_1^2 (y-1)^2} + \frac{2\hat{\lambda}_2}{\hat{\lambda}_1^3 (y-1)} \right) ds,
 \end{aligned}$$

$$I_7 = \int_{1/2}^1 \frac{1}{U_B^2} \left(\int_1^y U_B^2 ds_1 \right) ds,$$

$$D_0 = \alpha_0 \gamma_0 \lambda_1 I_2 - \frac{2\alpha_0 c_0 \lambda_2}{\lambda_1},$$

$$D_1 = \frac{2\alpha_0 c_0^2 \lambda_2}{\lambda_1^2} \left(\ln \left| \frac{c_0}{\lambda_1} \right| + \left(\frac{s_0 \lambda_1 \alpha_0^2}{s_0 \gamma_0^2 - c_0 \lambda_1 \alpha_0^2} \right) (1 + \ln \left| \frac{c_0}{\lambda_1} \right|) \right),$$

$$D_2 = \lambda_1 D_1 - c_0 D_0 - \left(\frac{\gamma_0^2 s_0 - \lambda_1 \alpha_0^2 c_0}{s_0 \alpha_0} \right) (\alpha_0 I_0 - 2c_0 + \gamma_0) - \alpha_0^2 \gamma_0 c_0 I_1,$$

$$D_6 = \alpha_0 \lambda_1 a_0 \left[\frac{s_0 \lambda_1 c_0}{s_0 a_0 - \lambda_1 c_0} \left(I_4 - \frac{1}{\lambda_1^2} \right) - \alpha_0^2 I_5 \right] - \frac{2\alpha_0 c_0}{\lambda_1},$$

$$D_7 = \frac{2\lambda_2 \alpha_0 c_0^2}{\lambda_1^2} \left[\frac{\lambda_1 c_0}{s_0 a_0 - c_0 \lambda_1} (1 + \ln \left| \frac{c_0}{\lambda_1} \right|) + \ln \left| \frac{c_0}{\lambda_1} \right| \right],$$

$$D_9 = c_0 D_2 - 2\alpha_0 c_0^2 \frac{\hat{\lambda}_2}{\hat{\lambda}_1} \ln \left| \frac{c_0}{\hat{\lambda}_1} \right| + \frac{s_0 a_0 c_0 I_2}{s_0 a_0 - c_0 \lambda_1} - \alpha_0 \gamma_0^4 \left(I_3 + \frac{1}{\alpha_0^2} \right) + 2\alpha_0 c_0 \gamma_0^2 I_1,$$

$$D_{10} = -c_0 D_6 + \lambda_1 D_7 + D_9 \left(1 - \frac{c_0 \lambda_1}{s_0 a_0} \right).$$

Acknowledgment

PS gratefully acknowledges the financial support from the University of KwaZulu-Natal. SSM and SS acknowledge support from the Norwegian Universities AID Programme, NUFU.

References

1. T.B. BENJAMIN, *Effects of a flexible boundary on hydrodynamic stability*, J. Fluid Mech., **9**, 513–532, 1960.
2. A.P. BASSOM and J. S.B. GAJJAR, *Upper-branch instability of flow in pipes of large aspect ratios with three-dimensional nonlinear viscous critical layers*, IMA J. Appl. Math., **42**, 119–145, 1989.
3. P. W. CARPENTER, *The effects of damping on the hydrodynamic stability of flows over Kramer-type compliant surfaces*, In laminar/turbulent boundary layers E.M. URAM and H.E. WEBER [Eds.], ASME, 53–59, 1984.
4. P. W. CARPENTER and J.S.B. GAJJAR, *A general theory for two- and three-dimensional wall mode instabilities in boundary layers over isotropic and anisotropic compliant walls*, Theoret. Compt. Fluid Dyn., **1**, 349–378, 1990.

5. P.W. CARPENTER and P. J. MORRIS, *The effect of anisotropic wall compliance on boundary layer stability and transition*, J. Fluid Mech., **218**, 171–223, 1989.
6. J.S.B. GAJJAR and P. SIBANDA, *The hydrodynamic stability of channel flow compliant boundary layers*, Theoret. Compt. Fluid Dyn., **8**, 105–129, 1996.
7. J.S.B. GAJJAR and F. T. SMITH, *On the global instability of free disturbances with a time-dependent nonlinear viscous critical layer*, J. Fluid Mech., **157**, 53–77, 1985.
8. R.D. JOSLIN, P.J. MORRIS and P.W. CARPENTER, *The role of three-dimensional instabilities in compliant wall boundary layer transition*, AIAA Jour., **29**, 10, 1603–1610, 1991.
9. R.E. KAPLAN, *The stability of laminar incompressible boundary layers in the presence of compliant boundaries*, Sc.D Thesis, MIT, 1965.
10. S.S. MOTSA, J.S.B. GAJJAR and P. SIBANDA, *The effect of heating/cooling on the upper-branch stability of boundary layer flows over a compliant boundary*, CAMES, **9**, 163–181, 2002.
11. J.M. ROTENBERRY and P.G. SAFFMAN, *Effect of compliant boundaries on weakly nonlinear shear waves in channel flows*, SIAM J. Appl. Math., **50**, 20, 361–394, 1990.
12. S. SHATEYI, P. SIBANDA and S.S. MOTSA, *Three-dimensional stability of heated or cooled accelerating boundary layer flows over a compliant surface*, ANZIAM J., **44**(E), E55–E81, 2002.
13. F.T. SMITH, *Nonlinear stability of boundary layers for disturbances of various sizes*, Proc. Roy. Soc. **A368**, 573–589, London 1979.
14. K. S. YEO, *The stability of flow over flexible surfaces*, Ph.D. Thesis, University of Cambridge, 1986.
15. K.S. YEO, *The stability of boundary layer flow over a single and multi-layer viscoelastic walls*, J. Fluid Mech., **196**, 369–408, 1989.
16. K.S. YEO, *The three-dimensional stability of boundary-layer flow over compliant walls*, J. Fluid Mech., **238**, 537–577, 1992.

Received June 2, 2003, revised version March 31, 2004.
